# Three-dimensional geostatistical modeling of subsurface stratification and SPT-N Value at dam site in South Korea

Mingi Kim[1a], Choong-Ki Chung[2b], Joung-Woo Han[2c] and Han-Saem Kim[*3]

*[1]Division of Urban Infrastructure Research, Seoul Institute of Technology,*
*37, Maebongsan-ro, Mapo-gu, Seoul 03909, Republic of Korea*
*[2]Department of Civil Environmental Engineering, Seoul National University,*
*1, Gwanak-ro, Gwanak-gu, Seoul 08826, Republic of Korea*
*[3]Earthquake Research Center, Korea Institute of Geoscience and Mineral Resources*
*124, Gwahak-ro, Yuseong-gu, Daejeon 34142, Republic of Korea*

**Abstract.** The 3D geospatial modeling of geotechnical information can aid in understanding the geotechnical characteristic values of the continuous subsurface at construction sites. In this study, a geostatistical optimization model for the three-dimensional (3D) mapping of subsurface stratification and the SPT-N value based on a trial-and-error rule was developed and applied to a dam emergency spillway site in South Korea. Geospatial database development for a geotechnical investigation, reconstitution of the target grid volume, and detection of outliers in the borehole dataset were implemented prior to the 3D modeling. For the site-specific subsurface stratification of the engineering geo-layer, we developed an integration method for the borehole and geophysical survey datasets based on the geostatistical optimization procedure of ordinary kriging and sequential Gaussian simulation (SGS) by comparing their cross-validation-based prediction residuals. We also developed an optimization technique based on SGS for estimating the 3D geometry of the SPT-N value. This method involves quantitatively testing the reliability of SGS and selecting the realizations with a high estimation accuracy. Boring tests were performed for validation, and the proposed method yielded more accurate prediction results and reproduced the spatial distribution of geotechnical information more effectively than the conventional geostatistical approach.

**Keywords:** 3D geostatistical model; 3D integration; conditional simulation; dam site; SPT-N; subsurface stratification

## 1. Introduction

For the reliable and economical design of infrastructure and evaluation of the geotechnical aspects of geohazards (e.g., landslides, subsidence, and earthquakes), the three-dimensional (3D) modeling of subsurface profiles and their geomaterial properties is essential. Such 3D modeling and visualization support 3D interactive visualization, provide useful interfaces, and aid spatial analyses of the subsurface (De-fu *et al.* 2008). Geotechnical spatial models have been developed using geostatistics and geometry, and the optimization of the workflow model in 3D modeling is crucial for the reliability and accuracy of geotechnical design and complex numerical modeling (Osterholt and Dimitrakopoulos 2007, De Rienzo *et al.* 2008, Chen *et al.* 2018). Spatial informatization is mainly dependent on two-dimensional (2D) or 2.5D (alternatively, pseudo-3D)

interpolation techniques in the horizontal direction of the geotechnical characteristic value of the engineering geo-layer, the standard penetration test (SPT), and the cone penetration test—particularly for predicting the regional cementation variability of soil deposits (De Rienzo *et al.* 2008; Kim *et al.* 2020).

For geotechnical 3D modeling, it is important to utilize all available geotechnical information. Each geotechnical investigation method has strengths and weaknesses in application. Although boreholes can provide accurate and deterministic geotechnical characteristic values, they cannot be used to obtain continuous subsurface information for a large construction area. Additionally, in-hole geotechnical tests (e.g., suspension P–S logging and downhole seismic testing) are relatively expensive and difficult to perform on a slope without site clearance; thus, it is difficult to establish a high-resolution geometry using only boring logs. In contrast, geophysical surveys (e.g., multichannel analysis of surface waves and electrical resistivity surveys) provide a 2D version of a 3D geophysical image or a computed-tomography scan of the entire construction site. However, geophysical surveys cannot be used for developing good stratigraphic profiling if the general stratigraphy consists of hard material over soft material, and they are only useful if the engineer or geologist is experienced with the testing method employed (Kim *et al.* 2020). Seismic exploration is

---

*Corresponding author, Ph.D.
  E-mail: adoogen@kigam.re.kr
[a]Ph.D.
  E-mail: mingikim@sit.re.kr
[b]Professor
  E-mail: geolabs@snu.ac.kr
[c]Master's Student
  E-mail: jwhan3@snu.ac.kr

primarily used to determine the subsurface stratification of engineering geo-layers to estimate the amount of soil used at construction sites and investigate rock discontinuity. Typically, seismic refraction tests involve exploration methods wherein artificial seismic waves are generated at the surface, and the refracting waves are observed. The waves returned at different geo-layer boundaries are analyzed to determine the thickness of the geo-layer or the velocity structure of the subsurface (Boschetti *et al.* 1996, Haeni 1986, Zelt and Barton 1998).

The geospatial characterization of geotechnical investigation results and parameters allows engineers to tackle the inherent complexity of the subsurface and perform regional geohazard assessments by using geostatistical interpolation to account for missing data (Sotiropoulos *et al.* 2016, Kim *et al.* 2016, Wang *et al.* 2021). Geostatistical methods have been widely used in geotechnical engineering to evaluate the spatial variability of the subsurface with limited measurements (Murakami *et al.* 2006, Zhang *et al.* 2013, Li *et al.* 2016). The accuracy of geostatistical methods depends on the stochastic/spatial distribution of the measured values even if the number of measurements is sufficient. In cases where the identification of stochastic/spatial correlations is difficult, the spatial interpolation and map production performance may be poor (McBratney *et al.* 2003, Grave *et al.* 2012). The most important precursor for reliable 3D geotechnical modeling of the entire construction site is optimization of the workflow of geostatistical estimations with consideration of the site-specific correlation of the geotechnical and geophysical properties. Techniques have been proposed that combine several geophysical survey results and one-dimensional data with engineering geo-layers obtained from multidimensional geometric constructions and/or geostatistical methods (Gómez-Hernández and Srivastava 1990, Oh *et al.* 2004, Gallerini and De Donatis 2009, Kim *et al.* 2012, Pinheiro *et al.* 2016).

A multivariate probability distribution is necessary to constantly couple design parameters and field/laboratory measurements for using the conditioning technique (Ching and Phoon 2014). The vertical and horizontal scales of the fluctuation for geo-layers and geotechnical index properties are affected by the inherent soil variability (Phoon and Kulhawy 1999); thus, the soil variability should be evaluated using statistical and geostatistical functions. Accordingly, trend removal methods, which are biased in estimating the variogram of a spatial variable exhibiting a trend, were proposed (Kim *et al.* 2016, Xu *et al.* 2021) for comparative testing using the conventional kriging method. Among the conventional spatial interpolation techniques, geostatistical techniques, such as kriging and simulation, have been widely used and have proven to be applicable to the spatial interpolation of various geotechnical properties. Recently, the standard guide for geostatistcal site investigation reports and selection of kriging/simulation approaches was published in ASTM D5549 (ASTM 2019) and primarily intended to report the environmental and geotechnical applications. Kim *et al.* (2016) proposed geostatistical 3D integration procedures for building a

geotechnical spatial grid by combining the geophysical tomography and boring log via indicator kriging (IK). To build a 3D structure with geo-layers assigned, the stiffness and bearing capacity of the geomaterial, along with the IK, which characterizes spatial variability using a nonlinear transform and indicator threshold, must be considered. Nevertheless, prediction residuals obtained via trial-and-error approaches for determining the optimum geo-layer criteria result in an unreliable structure of the 3D geo-layers.

However, kriging techniques are focused on smoothing the original dataset's intrinsic distribution owing to a measurement procedure that reduces the variance of error; thus, they overestimate small values and underestimate large values. A conditional simulation (e.g., sequential Gaussian simulation (SGS)) is an effective method of solving ordinary kriging (OK) deficiencies by transforming the actual data into Gaussian data. This is a stochastic method for estimating the forecast by generating a random field, preserving the known values at the sampling points, and providing constraints for reducing the uncertainty in subsurface stratification (Huang *et al.* 2019). The conditional simulation results vary according to the generation of random numbers and the simulation time.

There is no quantitative measure of the reliability of each simulation result. Therefore, a new optimization approach is needed to realize the geostatistical integration of site survey data, and a geographic information system-based integration system should be developed to automate this optimization procedure. The conditional simulation technique has the disadvantage of reproducing multiple stochastic realizations. This is because the realization of the conditional simulation depends on the random path and the generated random number. As there have been few attempts to evaluate the reliability of multiple realization results in the past, the final prediction was determined by averaging all the realization results, i.e., as the simulation mean (e-type estimate).

In this study, a 3D geostatistical modeling procedure for borehole and seismic refraction tests that involves comparing the cross-validation-based prediction residuals was developed and applied to a dam emergency spillway site in South Korea. By applying a 3D geospatial database and optimization of geostatistical interpolation techniques, the site-specific 3D geometric information of the subsurface stratification and SPT-N value were predicted. First, site-specific P-wave velocity ($V_P$) values were derived locally for each geo-layer boundary by supplementing and modifying the integration method developed by Kim *et al.* (2016). In contrast to the conventional integration method, an optimization procedure involving OK and SGS was applied. Second, SGS-based optimization of the SPT-N value via 3D modeling was implemented. The proposed methods are aimed at realizing the 3D mapping of the geotechnical engineering properties at the dam site, while considering the spatial uncertainty and locality of the geotechnical testing results on a steep slope. Test boring logs guaranteeing the actual geo-layer and SPT-N value were compared with the 3D modeled geometry to verify its accuracy

Fig. 1 Plan view of the borehole location and seismic refraction test lines at a dam-emergency-spillway construction site in Gyeongsangbuk-do, South Korea

## 2. 3D geospatial database

### 2.1 Study area

3D geotechnical spatial modeling of the dam-emergency-spillway construction site located in Gyeongsangbuk-do, South Korea was performed. The dam, which was completed in 1976, is a multipurpose dam located upstream of the Nakdong River. Owing to the impact of heavy rainfall due to climate change, wall-mounted open-type emergency spillway construction was initiated to increase the storage capacity and ensure the safety of the dam. It was completed in 2014, after 7 years of construction. Slope failure occurred several times during the construction owing to the joint of the rock mass. The proposed 3D modeling was used to simulate the initial ground condition using the geotechnical investigation information in the design phase, and the obtained results were used as supplementary data for a careful review of the geotechnical and geological safety.

The design of geotechnical engineering in sensitive land formations with little knowledge of subsurface profiles is a common reason for failure. The engineering geological properties of the subsurface comprising the dam basement should be investigated to identify probable problems and appropriate precautionary measures (Kocbay and Kilic 2006). Neglecting the subsurface profile can cause stability issues during construction management (Kim *et al.* 2016). With regard to economic and performance-based design, understanding the site-specific subsurface stratification and related geotechnical parameters is essential for estimating the excavation depth and bearing capacity of the spillway. Fig. 1 shows the locations of the boreholes and seismic refraction tests performed at the construction site. The number of boreholes in the target area was 41, and the number of seismic refraction test lines was 12. For the validation of the 3D modeled profiles in certain regions through comparison with actual measurements, two and

three boreholes were randomly selected and omitted from the 3D geostatistical interpolation of the subsurface stratification and SPT-N value, respectively. In Fig. 1, the line A-A' is the centerline of the dam-emergency-spillway site corresponding to the cross-sectional view (Fig. 11) of the 3D geometry of subsurface stratification.

### 2.2 Borehole information without outliers

The engineering geo-layer strata are categorized into seven groups: landfill, alluvium, weathered residual soil, weathered rock, soft rock (denoted as engineering bedrock), moderate rock, and hard rock (Kim *et al.* 2016). Because the soil deposit in the target area was not sufficiently thick to distinguish the soil layer boundary, detailed classification of the soil deposit, such as the boundary of the landfill and alluvium, was not performed. The site-specific criteria of $V_P$ corresponding to the engineering geo-layer strata were defined to distinguish the rock boundaries: (1) the depth to weathered rock refers to the boundary layer between the soil layer and weathered rock; (2) the depth to soft rock refers to the boundary layer between the weathered rock and soft rock. At the target boundary of the engineering geo-layer with the boreholes, the depths to the weathered rock and soft rock are distributed in 3D space (Fig. 2(a)).

The SPT detailed in ASTM D 1586 (ASTM 2002) provides the penetration resistance related to the blow count (N-value), which is widely used to determine engineering properties and soil design parameters. The sampler is first driven to a depth of 15 cm below the bottom of the pre-bored hole, and then the N-value is adjusted to drive the sampler another 30 cm into the soil. After the N-value was extrapolated linearly according to 50 blow counts, 102 points (i.e., extrapolated N-value depended on penetration depth) with an N-value of ≥150 were excluded from the spatial interpolation. This is because the reliability of the correction formula for the energy-corrected N value (i.e., $N_{60}$) and the normal score transformation for OK and SGS
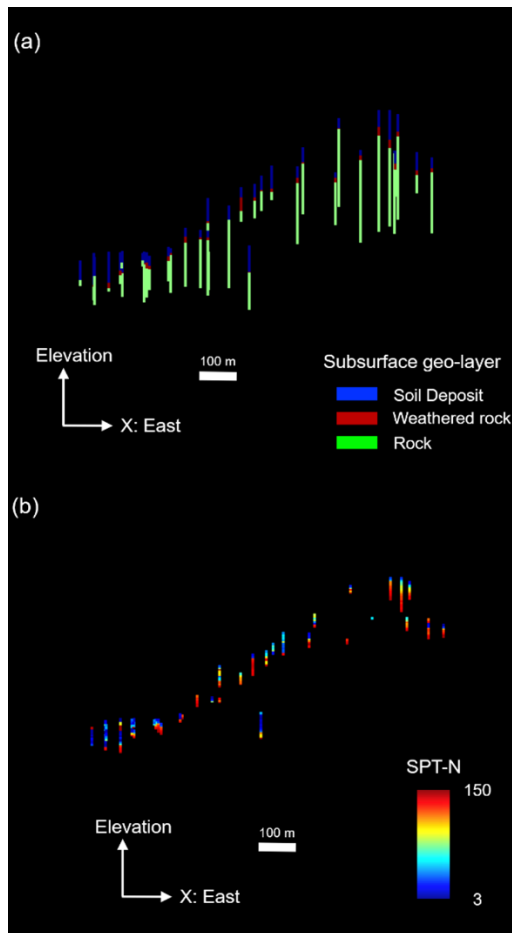
Fig. 2 2D sectional distribution of the borehole-based profile with (a) the engineering geo-layer and (b) SPT-N along the line A-A' in Fig. 1
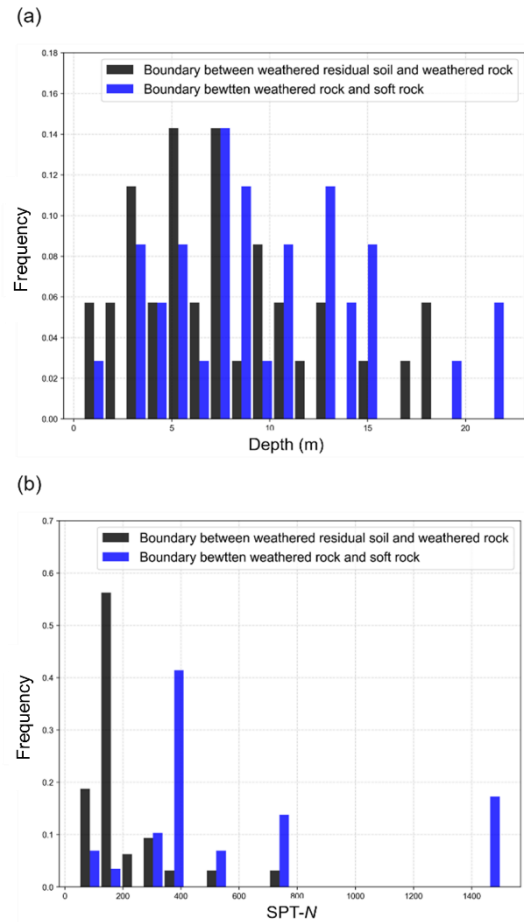


Fig. 3 Histogram of the (a) depth and (b) SPT-N value at the boundaries between weathered residual soil and weathered rock and between weathered rock and soft rock

cannot be guaranteed when N ≥ 150 (Kim *et al*. 2020). Through the linear extrapolation, the notation was unified when the N-value was ≤50 and when it was ≥50, and the geostatistical interpolation technique for continuous variables could be applied. N-values from 239 points along the test depth of the 37 boreholes were used for the spatial interpolation (Fig. 2(b)). As the SPT results differ with regard to the energy efficiency delivered depending on the equipment, the N-values can obtained differently even under the same geotechnical and geological conditions. To correct the results of the field N-value with 60% of the energy efficiency (EE), the correction formula $N_{60} = (EE/60) \times N$ was applied. Cases where the bearing capacity was under- or overestimated were eliminated, and the $N_{60}$ value used in the empirical formula was calculated for deriving other geotechnical parameters. The N-value refers to the linearly extrapolated $N_{60}$ value (Kim *et al*. 2020).

The depth to the target rock boundaries with boreholes and the SPT-N value at this depth are presented in the histogram of Fig. 3. The depth to the weathered rock was mainly distributed at 3, 5, and 7 m, and the depth to the soft rock was relatively biased toward a larger depth of >7 m. The extrapolated N-values at the depth of weathered rock were concentrated at 150. The extrapolated N-values at the depth to the soft rock were concentrated at 400.

The borehole dataset may include outliers owing to the spatial uncertainty of the underlying geological formation, inconsistent testing equipment and methods, and human errors. For stochastic and geospatial characterization based on interpolation of the borehole datasets, a borehole dataset with outliers can be excluded from the 3D geospatial assessment. Among the various outlier detection and analysis methods, the outlier analysis method based on cross-validation (Kim *et al*. 2012, 2016) was applied in this study. This method involves the comparison of the experimental value with the value obtained using the kriging method for all the boreholes. Cross-validation is a test for determining the consistency of variogram or kriging models (e.g., simple kriging (SK)) (Delfiner 1976, Guarascio *et al*. 1976, Isaaks and Srivastava 1989). The calculated properties were tailored for the measurement of local reliability using a sequential blind test. Accordingly, the outlying borehole datasets were detected, and the measured and estimated values were compared via cross-validation.

Fig. 4 shows the correlations between the observed and predicted geo-layer depths based on cross-validation for each borehole location. The depth to weathered rock and the depth to bedrock were selected as the attributes to be
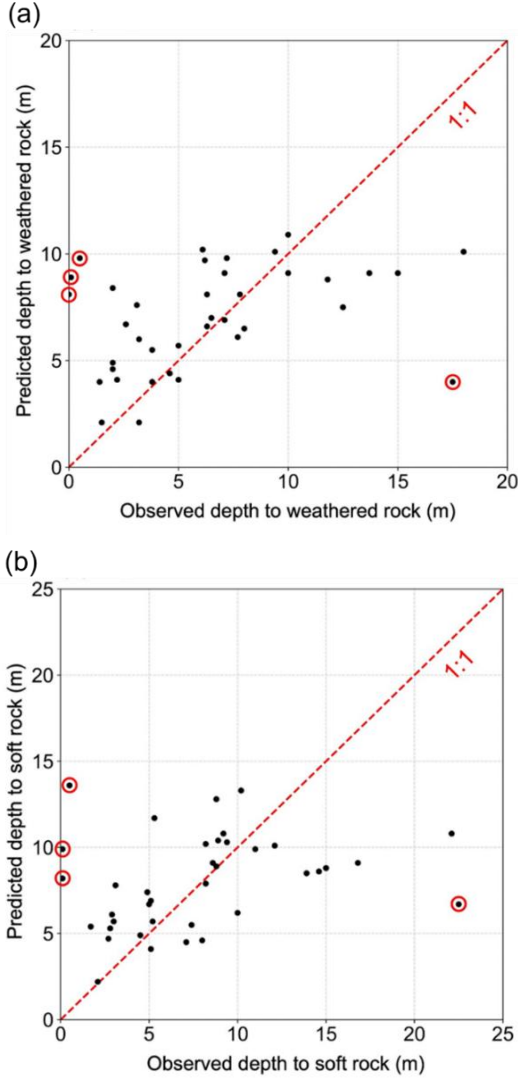
Fig. 4 Outlier analysis results for the (a) depth to the weathered rock layer and (b) depth to the soft rock layer; the red circle indicates the outliers for the depth to each geo-layer



Fig. 5 3D distribution of the seismic refraction test: (a) digitized P-wave velocity ($V_P$); (b) 3D geometry of $V_P$ interpolated using OK

compared. SK was used to predict the geo-layer elevation of each excluded borehole point using the following equations (Wackernagel 2003):

$$\hat{\gamma}(h) = \frac{1}{2h} \sum_{i=1}^{n} (Z(x_i) - Z(x_i + h))^2 \qquad (1a)$$

$$\hat{Z}(x_0) = \sum_{i=1}^{n} \lambda_i Z(x_i) + \left[ 1 - \sum_{i=1}^{n} \lambda_i \right] \mu \qquad (1b)$$

where $\hat{\gamma}(h)$ denotes the semi-variogram, $\hat{Z}(x_0)$ represents the estimated value of an attribute at the point of interest $x_0$, $Z(x_i)$ represents the observed value at the sampled point $x_i$, $\lambda_i$ is the weight assigned to the sampled point, $n$ represents the number of sampled points used for the estimation, and $\mu$ is a known stationary mean, which was set as the average data constant for the entire domain (Webster and Oliver
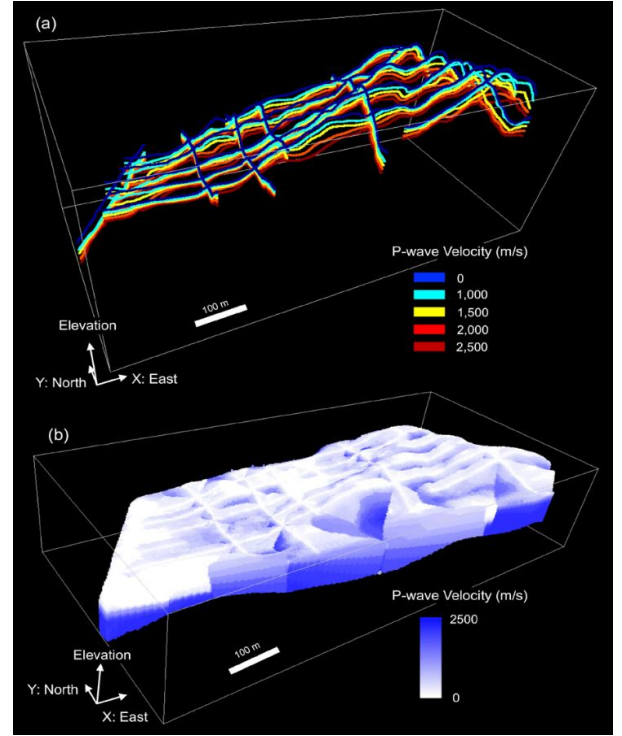
2007). The $\hat{Z}(x_0)$ values are each considered to be a realization of $Z$ at position $i$. There is a probability distribution for each random variable $\hat{Z}(x_0)$. In this study, second-order stationarity was assumed in the variogram and kriging, according to the following rules: (1) the estimation and variation of $\hat{Z}(x_0)$ are constant; (2) the covariance between $Z(x_i)$ and $Z(x_i + h)$ only relies on the distance $h$ between the observations and not on the spatial location $x_i$. On comparing the cross-validation errors at each point, four boreholes, corresponding to the least reliable 10% (Kim *et al.* 2012) of the total 41-borehole dataset, were assumed to contain outliers and were excluded from the 3D modeling procedure. The boreholes at the same points were classified as outliers of the depth to weathered rock and depth to bedrock (i.e., soft rock).

### 2.3 Digitized V_P profile

Because the digital data of the travel-time curves were not included in the site survey reports, the digitization of the tomography images was performed in three steps (Kim *et al.* 2020)

1. Determining the grid cell size (e.g., 1 m or 5 m) and gridding;
2. Overlapping the grid onto the tomography image of $V_P$;
3. Digitizing the $V_P$ contour and assigning the velocity value at each grid cell.

The seismic velocities designated as the tomography contours were 0, 1000, 1500, 2000, and 2500 m/s. The digitized results, which were the (x, y) coordinates and the
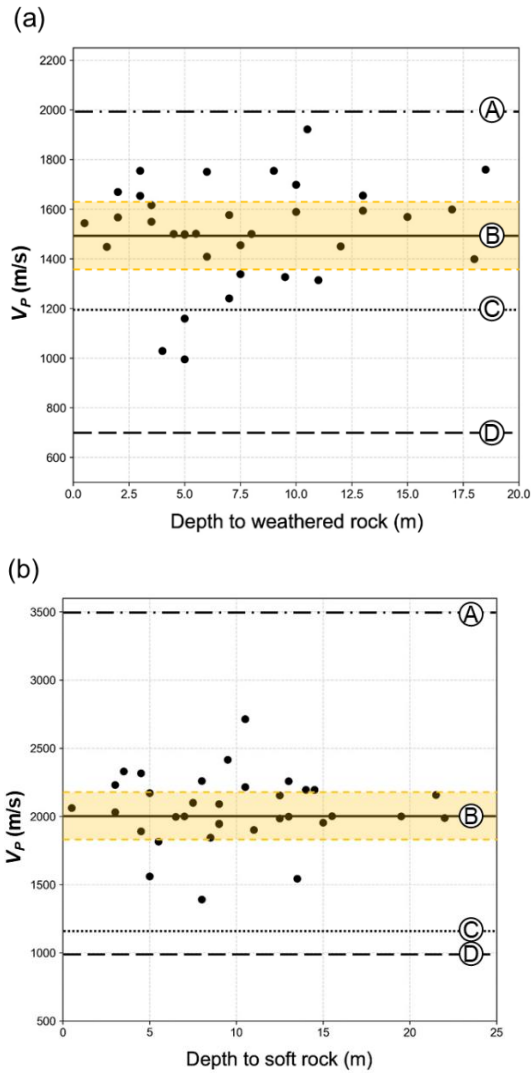
(a)



(b)



Fig. 6 P-wave velocity ($V_P$) at (a) the boundary between the weathered residual soil and weathered rock and (b) the boundary between the weathered rock and soft rock, at the seismic refraction test lines that coincided spatially (within 5-m spacing) with the boreholes
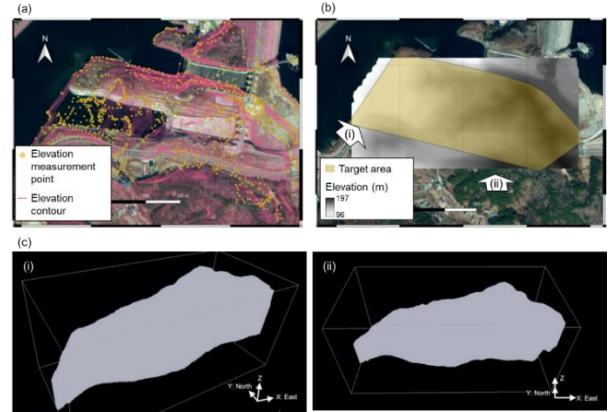


Fig. 7 Procedure for obtaining the DEM-based unstructured 3D grid: (a) location of the elevation survey and contour data, (b) generated DEM and vector polygon layer of the target area, (c) 3D unstructured grid volume (without shading effect) generated from clipped DEM: the southwestern direction (i) and southern direction (ii)

Corporation 2002). The yellow boxes are within 1 standard deviation of the mean of $V_P$ with the target boundary. The $V_P$ values at the depths to weathered rock and soft rock were distributed within 1200−1800 m/s (mean: 1520 m/s) and 1500−2500 m/s (mean: 2082 m/s), respectively, which were found to most closely resemble the $V_P$ criteria (1500 and 2000 m/s for the target rock boundaries) in the geotechnical investigation handbook of Seoul Metropolis (B in Fig. 6) among the domestic criteria for geomaterial classification based on $V_P$. As a result, the best-fitted $V_P$ criteria (B in Fig. 6) were used to initially assume the reference correlation of $V_P$ and target rock boundary as the first step in Fig. 8.

### 2.4 Digital elevation model-based unstructured 3D grid

The unstructured grid is the most general form of a dataset defining a subsurface volume and has been used to solve problems involving complex geometries. In this study, a digital elevation model (DEM) representing the terrain topology was generated using global positioning system-based elevation survey data and the contour lines of a digital map (Fig. 7(a)). A spatial grid with a resolution of 2 m was formed with a matrix of cells arranged in rows and columns. The value of each cell was spatially assigned using the interpolated subsurface stratification and SPT-N value. The rasterize function from QGIS was used to convert vector data into raster data. Subsequently, a vector polygon that covered the seismic refraction test lines was constructed (Fig. 7(b)). Only the overlapping region of the DEM and the polygon was clipped. According to the clipped DEM, vertical cells were generated from the ground level to a depth of −50.0 m. An unstructured grid volume was constructed for the model to include 100 cells of 0.5 m for each point on the floor plan. Fig. 7(c) presents the 3D target grid volume for the modeling generated from the clipped DEM. The unit size of the grid volume was 2 m in the horizontal direction and 0.5 m in the vertical direction.

elevation corresponding to each $V_P$, were stored in the geospatial database. Fig. 5 presents the 3D distribution of the $V_P$ value, which was digitized and spatially interpolated via OK. The $V_P$ value was higher toward the northeast (up to 2000 m/s), where outcrops existed locally (Fig. 3(a)), and lower toward the southwest (up to 800 m/s). The soil layers in the southwest area, which primarily comprised silty clay, were accumulated through fluvial sedimentation and formed by unconfined geomaterials with low SPT-N (<15) and $V_P$ (<1000 m/s).

$V_P$ was extracted at the target rock boundaries with boreholes, spatially coincident (within 5-m spacing) with the seismic refraction test lines. As shown in Fig. 6, for determining the site-specific $V_P$ criteria, the following domestic criteria of the geomaterial classification based on the P-wave velocity were compared: A (Korea Highway Corporation 2009), B (Seoul Metropolis 2006), C (Korea Train Express Corporation 1995), and D (Korea Land

# 3. 3D geospatial interpolation of subsurface stratification

## 3.1 Framework for optimized 3D integration

Trials have been conducted to evaluate the correlation between the 2D subsurface $V_P$ profiles and the borehole-based characteristic value. However, it was difficult to establish and apply the correlation at the steep construction site owing to its large subsurface variability arising from the separation distance between the borehole locations and the seismic refraction test lines. Kim *et al.* (2016) proposed a geospatial data integration method comprising the use of IK and cross-validation with the aim of determining the local optimal $V_P$ for the classification of geomaterials. Herein, we propose a method for improving the reliability of the integration results by applying SGS with the following two modifications. First, a 3D geostatistical interpolation method was adopted to calculate the 3D volume of the $V_P$. In the previous integration method (Kim *et al.* 2016), the 2D elevation maps of each $V_P$ were stacked. This is a type of 2.5D interpolation method and has a limitation in capturing the trend of 3D spatial variability—particularly in the vertical direction. The second modification was the implementation of a SGS as a geostatistical method. Kriging derives one optimized linear estimation result, but it is difficult to estimate the extreme values, owing to the smoothing effect. Moreover, the interpolation result is significantly affected by the spatial bias of the dataset (Delfiner 1976).

We used two geostatistical methods—OK and SGS—as representative conditional simulation techniques. A subsurface stratification method was developed in this study to determine the method with higher reliability between OK and SGS. For OK, a stationary assumption (Li *et al.* 2000) or underlying assumption, that is, a constant expectation, should be fulfilled in the entire field or at least a sampling field. OK presumes that the error between predicted and observed values should be minimized when determining the kriging weight ($\lambda_i$ in Eq. (1b)) and that the estimated value is unbiased. The distribution of a simulated point or grid is assumed to be normal in an SGS. Its mean and variance are the prediction value and error variance calculated via SK. It can predict the given dataset using a normal distribution. Preprocessing, e.g., using a normal score or a lognormal transform, is required if the distribution of the experimental data is not normal (Kim *et al.* 2020). SGS sequentially generates $N$ data and thus reproduces the distribution and covariance of the original data collection. The variable $z_1$ is generated using the random variable $z$ given by $n$. In the next step, another variable $z_2$ is generated by assuming that $z_1$ is included in the original dataset. This procedure is repeated until $N$ data are produced for the sequential simulation. The procedure can be represented as an equation with a repeated conditional probability, as follows

$$f(n) = f((N-1) \cup n) \cdots f(n);$$
$$(n-1) \cup n = \{(N-i): generated\ data\} \cup \{n: given\ data\}, \quad (2)$$
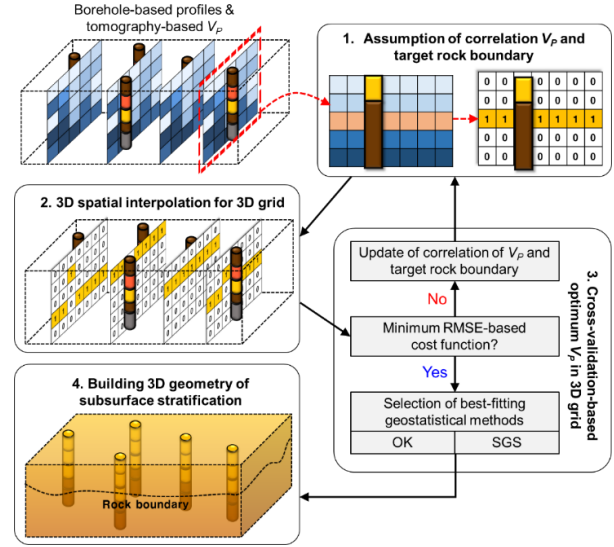


Fig. 8 Schematic of the subsurface stratification method involving optimized 3D integration of the borehole-based depth to geo-layers and seismic refraction test-based $V_P$

where $(N-1) \cup n$ denotes the union of $(N-i)$ generated data, and $n$ denotes the given data. This implies that the $(N-i+1)^{th}$ datum is generated while assuming that the data already generated are known for the next calculation.

Fig. 8 presents the procedure of the subsurface stratification method for the integration of the borehole-based strata and tomography-based $V_P$. For this analysis, the following workflow was used for stepwise optimization: (1) a correlation $V_P$ was assumed with a target rock boundary based on the reference correlation; (2) 3D spatial interpolation was performed with OK and an SGS for the assumed boundary; (3) cross-validation of the interpolated 3D geometry with the measured rock boundary in the borehole datasets was performed; (4) steps 2 and 3 were repeated until the cross-validation-based root-mean-square error (RMSE) was minimized to build a 3D geometry of the target rock boundary using the best-fitting geostatistical methods. The optimization phase involves a process of iteration for defining the site-specific optimum $V_P$-based rock boundary and the application of geostatistical methods. A QGIS plugin was designed and used to automate the optimum $V_P$ calculation method.

## 3.2 Site-specific classification criteria within $V_P$

The reference values of $V_P$ recommended in the geotechnical investigation handbook of Seoul Metropolis are 1500 m/s for the depth to weathered rock and 2000 m/s for the depth to bedrock for the closest agreement with the actual $V_P$ at the target rock boundaries (Fig. 6). However, the $V_P$ value is generally different from the actual field velocity, because it is significantly affected by the density and Young's modulus of the subsurface. Therefore, it is necessary to use an optimized $V_P$ for the field conditions based on the data-driven method, which can be calculated via a comparison with the interpolated depth to geo-layers.

An initial value was assumed for calculating the

optimum $V_P$ at the depth of weathered rock. The initial reference value was set as 1500 m/s, and the depths to the weathered rock were obtained along the test lines from the digitized $V_P$ profile (Fig. 5(a)) of the 3D geospatial database. Then, among the 37 boreholes (after removal of 4 outliers from 41 boreholes), the interpolation of the assumed depth to weathered rock along with the $V_P$ test lines and the experimental depth for 36 of the boreholes yielded the predicted value of the depth to weathered rock of the excluded borehole. The procedure was repeated for 36 boreholes, and the error between the predicted and measured values was determined as the RMSE. The RMSE values were obtained by assuming the $V_P$ at the depth of the bedrock to be 3/5, 3/4, 7/8, 6/5, 5/4, and 9/8 of the initial value of $V_P$. OK and SGS were applied for the 3D geospatial interpolation of the assumed depth to weathered rock along the $V_P$ test lines and the measured value of the borehole dataset.

Among the predicted depths to the two rock layers for the assumed $V_P$ criteria of OK and SGS, the $V_P$ with the smallest RMSE was determined as the optimum $V_P$. Fig. 9 shows the RMSE according to the $V_P$ and the polynomial regression line (using quadratic equations), which was obtained to calculate the optimum $V_P$ with the minimum RMSE. According to the seven assumed $V_P$ values, the RMSE were obtained by integrating with borehole data through cross-validation. The optimization method based on OK exhibited better prediction performance and smaller RMSE values than that based on SGS for the subsurface stratification of the depth to weathered rock (i.e., the boundary layer between the soil deposit and weathered rock). The minimum RMSE was 2.78 m when the $V_P$ value was 1346.91 m/s. The minimum value of the obtained quadratic equation was 2.8 m when the $V_P$ value was 1369.29 m/s. These values are smaller than the reference value of 1500 m/s. The use of the proposed method is expected to reduce the prediction error for the boundary layer between the soil deposit and weathered rock by approximately 0.21 m.

The proposed method with SGS exhibited better prediction performance, with a smaller RMSE, than that
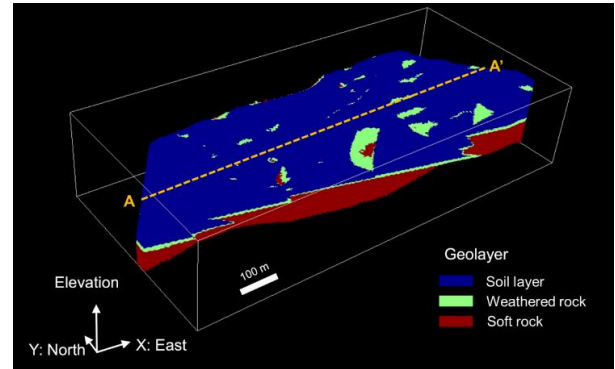


Fig. 10 3D geometric information with the subsurface stratification in the target area; the line A–A' was distributed for the cross-sectional view (Fig. 11) of the stratification with the verification borehole points (Fig. 1)

with OK for the subsurface stratification of the depth to bedrock (i.e., the boundary layer between the weathered rock and soft rock). The minimum RMSE was 1.69 m when the $V_P$ value was 2001.49 m/s. The minimum value of the determined quadratic equation was 1.79 m when the $V_P$ value was 1868.62 m/s. There was no significant difference between the results of the proposed optimization method and the reference values in this case. Thus, the 3D subsurface information of stratification was constructed and visualized according to the best-fitted local correlations of $V_P$ and the target rock boundaries (Fig. 10). In general, the depths to weathered rock and soft rock were more deeply dispersed to the northwest and shallower to the east, where there were local outcrop rocks. Owing to the thin soil layer and weathered rock layer, despite the high spatial variability, it was difficult to distinguish the boundary when only the reference $V_P$ of the rock boundary was used. The best-fitted $V_P$ correlations were useful for examining the small variation of the rock boundary in the high-resolution 3D geometry, which comprised a 3D square grid (x-y-z plane) with a unit grid size of 2 m × 2 m × 0.5 m.

### 3.3 Verification of 3D geometric information of subsurface stratification

After calculating the optimum $V_P$ of the boundary of geo-layers, we defined three borehole datasets as test datasets for the cross-validation to verify the accuracy of the proposed method. Among the 37 boreholes that were found to have no outliers, 3 were selected as the test boreholes. They were selected from the dataset used by Kim *et al*. (2016) to compare the reliability of the original method and the proposed method. The $V_P$ criterion adopted for the determination of the depth to weathered rock was 1346.91 m/s, and that of the bedrock was 2001.49 m/s, both of which had the smallest RMSE (Fig. 9). For the stratification of the depth to weathered rock, the elevation obtained from the $V_P$ and that of the borehole dataset were interpolated via SGS. Correspondingly, the transformed elevation obtained from the $V_P$ and that of the borehole dataset were interpolated using OK.
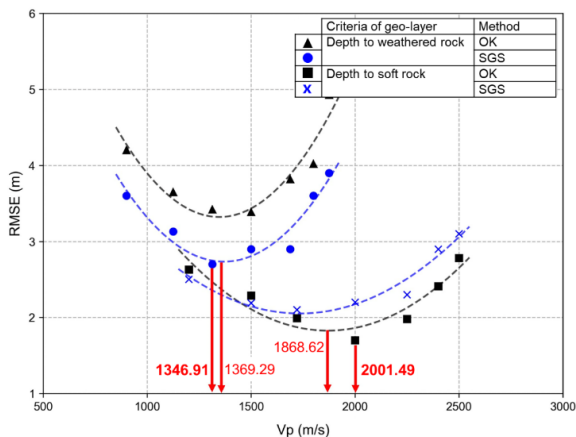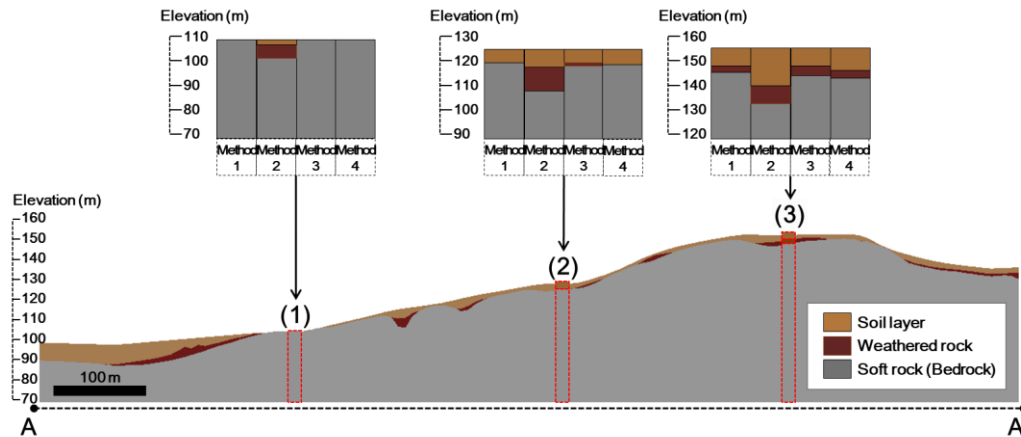


Fig. 9 Locally specified $V_P$ classification criteria at the depth to weathered rock and depth to soft rock for the methods based on OK and SGS

Fig. 11 Comparison of the experimental values and prediction results for the test boreholes (1)–(3) and cross-sectional view along the line A–A' (Fig. 1) based on the proposed 3D integration method; method 1 involved the geo-layer profile from the validation boreholes, method 2 involved the use of SK only with the geo-layer in the borehole datasets, method 3 involved the 2.5D integration results (Kim *et al*. 2016), and method 4 involved the proposed 3D integration

A cross-sectional view of the interpolated geo-layer was extracted along the centerline of the vector polygon layer in the target area by applying the proposed subsurface stratification method (Fig. 11). The experimental boundary from the borehole dataset was compared with the prediction results of the three methods. The first method employed the geo-layer profile obtained for the three validation boreholes (Fig. 1). In the second method, the geo-layers were predicted by applying SK for only borehole-based geo-layers. In the third method, the geo-layers were predicted using the IK-based geospatial integration method presented by Kim *et al*. (2016). In the fourth method, the geo-layers were predicted using the proposed approach.

For all the test boreholes, the prediction performance of the second and third methods was better than that of the first method, according to a comparison of the results with the geo-layer boundary of the three-borehole dataset. For boreholes (1) and (2), the predicted geo-layers of the second and third methods were similar. For borehole (3), i.e., the second method, the integration method of Kim *et al*. (2016) exhibited better prediction performance than the proposed integration method. This is because the overall RMSE values were smaller than or similar to those of the integration method (Kim *et al*. 2016). When IK was employed as a spatial interpolation method, the overall RMSE was >4.0 m for the depth to weathered rock (2.78 m of RMSE in this study). Thus, it was confirmed that the application of the proposed method using OK and SGS simultaneously provided higher reliability for predicting subsurface stratification in the entire construction area rather than SK and IK.

## 4. 3D geospatial interpolation of SPT-N value

### 4.1 Framework for optimization of SGS

The SGS procedure was optimized for the geostatistical interpolation of the SPT-N value (Fig. 12). The proposed
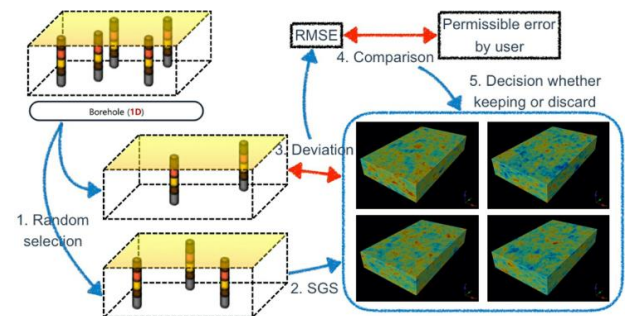


Fig. 12 Schematic of the optimized 3D geospatialinterpolation method with the application of SGS

SGS optimization method aims to determine the reliability of multiple realizations of the SGS quantitatively with the use of only results with realizations having a high reliability and constant spatial tendency. Engineers have endeavored to choose the best method from various spatial interpolation methods and to calculate and reduce the prediction error that occurs with the application of that method. However, the proposed optimization method allows geotechnical engineers to select and use the prediction result with the desired prediction performance. The reliabilities of multiple realizations of the SGS are calculated using a cross-validation approach. The first step is to exclude a certain number of boreholes. The second step is to perform the 3D geostatistical interpolation of the SPT-N values that have not been excluded by SGS (or sequential indicator simulation (SIS) (Kim *et al*. 2020)) and to obtain one embodiment. Third, the SPT-N profiles of the excluded boreholes are compared with those estimated from the realization result of the corresponding locations and depths, and the deviation is calculated. Fourth, the RMSE is compared with the permissible error set by the engineer. If the RMSE exceeds the permissible error, the realization result is retained; otherwise, it is discarded. Finally, the retained realization results with high prediction accuracies are averaged, yielding the final spatial interpolation result.
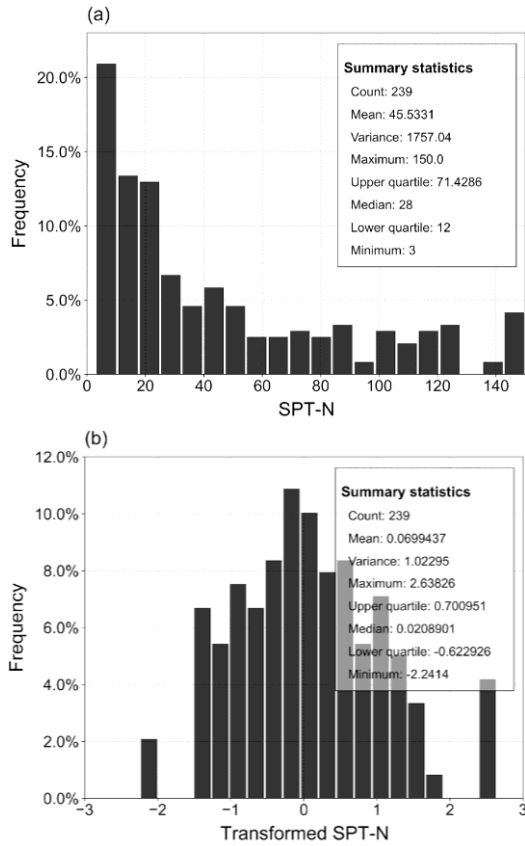
Fig. 13 Histogram and summary statistics of the (a) extrapolated SPT-N value and (b) normal score transformed SPT-N value
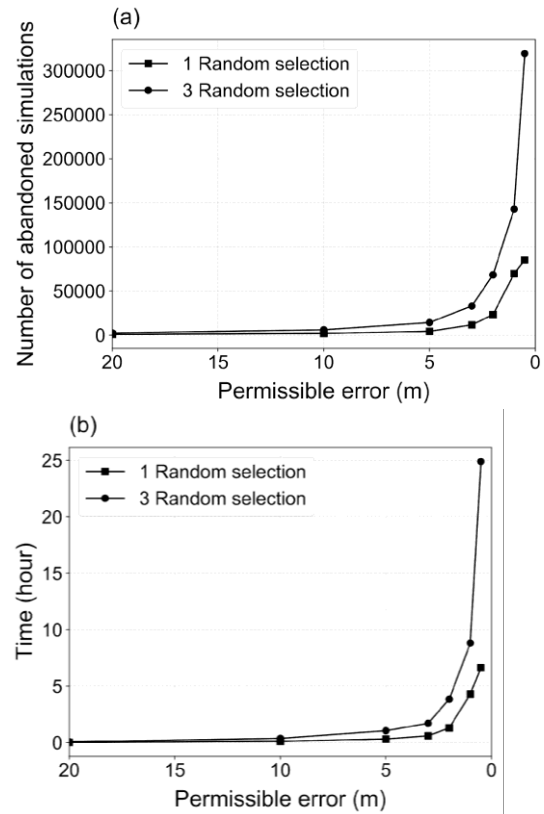


Fig. 14 (a) Number of abandoned simulations and (b) computing time with respect to the permissible errors and the number of selected boreholes in the geostatistical optimization procedure

The dependent variables of the optimization method include the number of excluded boreholes, user-defined permissible error, and number of realizations for the e-type estimate. The expected values of the normalized SPT-N value were obtained via stochastic and iterative simulations and transformed into the experimental N values. The e-type approach, which is the most commonly used post-processing method, obtains the final prediction result by averaging the simulation results using the grid location (Kim *et al*. 2020). The independent variables of the optimization method include the number of realizations discarded during the iterative process and the computation time for the entire process. It is essential to automate the optimization procedure because the procedure must be iterated until the desired result is obtained. Among the various conditional simulation methods, SGS is adopted to simplify the iterative automation. In contrast to SIS, which requires nuerous user-setting values, such as indicator thresholds, SGS requires only the minimal settings, similar to variogram modeling. Accordingly, the optimization procedure was automated using R—a programming language specialized for statistical operations—and "gstat," which is a geostatistics package of R. This module was produced in the form of a QGIS plugin.

### 4.2 3D geometric information of SPT-N value

A normal score transform was applied because the

Table 1 Application cases of the optimization method for 3D spatial interpolation of SPT-N

| Case | Number of excluded boreholes | Permissible error |
|------|------------------------------|-------------------|
| 1 | | 0.5 |
| 2 | | 1 |
| 3 | | 2 |
| 4 | 1 | 3 |
| 5 | | 5 |
| 6 | | 10 |
| 7 | | 20 |
| 8 | | 0.5 |
| 9 | | 1 |
| 10 | | 2 |
| 11 | 3 | 3 |
| 12 | | 5 |
| 13 | | 10 |
| 14 | | 20 |

histogram distribution of the extrapolated N-value did not follow the normal distribution (Fig. 13(a)). The transformed N-values were interpolated using the optimized SGS procedure, and the back normal score transform was applied to the final prediction result for the independent variables in
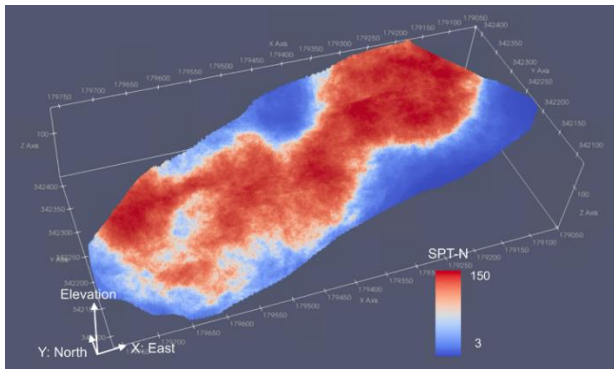
Fig. 15 3D geometric information assigned with SPT-N values according to the optimization method of SGS when the number of excluded boreholes is 3 and the permissible error is 0.5

14 cases (Table 1). The number of realizations for the e-type was fixed at 100 to examine the sample statistics reproduction for all generated realizations (Leuangthong *et al.* 2004).

Fig. 14(a) presents the number of abandoned simulations with respect to the permissible error and the number of selected boreholes during the iterative process. As the user-defined permissible error increased, the number of abandoned simulations increased. As the permissible error decreased, the number of abandoned simulations increased. When the optimization was performed under the condition that the number of excluded boreholes was 3 and the permissible error was 0.5, more than 300000 realizations from the SGS were discarded to obtain 100 optimized realizations. This indicates that the conventional SGS uses only the 1st to the 100th realizations, whereas the optimization technique requires many more simulation results. Fig. 14(b) presents the correlation between the computing time for the iterative process and the number of excluded boreholes and permissible error. As the number of excluded boreholes increased, the computing time increased. As the permissible error decreased, the computing time for the analysis increased. When the optimization was performed under the condition that the number of excluded boreholes was 3 and the permissible error was 0.5 using a desktop computer with a 3.8-GHz Intel Core i5 CPU and 24 GB of random-access memory, the geospatial interpolation required >25 h. The 3D geometric information of the SPT-N (Fig. 15) value was generated via the optimization of SGS (i.e., e-type of 100th realization) under the condition that the number of excluded boreholes was 3 and the permissible error was 0.5.

### 4.3 Verification of 3D geometric information of SPT-N value

Two test boreholes (a) and (b) (Fig. 1) were used to confirm the reliability of the optimized SGS-based 3D geometric information of the SPT-N value. The SPT-N profiles at location of the test boreholes were predicted via the proposed method and OK, and the results were compared with the actual SPT-N values. The geostatistical optimization was performed under the condition that the
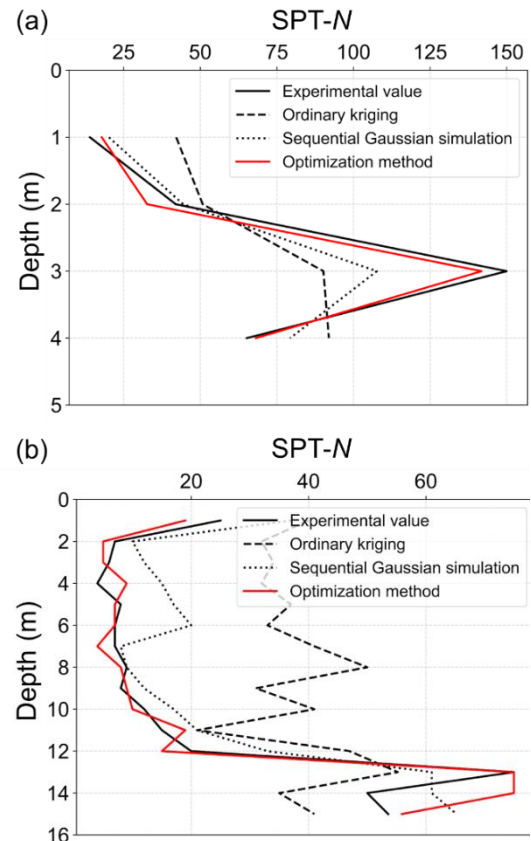


Fig. 16 Reliability test results obtained with two test boreholes: 3D spatial interpolation results obtained using the proposed optimization method, OK, and SGS

number of excluded boreholes was 3 and the permissible error was 0.5. For both test boreholes, the SPT-N profiles predicted via the proposed optimization procedure were the most likely to resemble experimental N value; thus, they were more accurate than those of OK and SGS. The spatial tendency of the SPT-N value with respect to the depth was accurately reproduced using the proposed method (Fig. 16).

## 5. Conclusions

We performed 3D modeling of the geotechnical information in a dam-emergency-spillway construction site, where slope failure occurred several times during the construction. The 3D subsurface geo-layer strata and spatial distribution of the SPT-N value were predicted using borehole-based profiles and tomography-based $V_P$. Geostatistical techniques were modified and applied in terms of geotechnical and geological engineering for the geospatial interpolation of the site investigation information. The modified method can provide site-specific interpolation results for overcoming the spatial uncertainty of biased and sparse geotechnical information. $V_P$ profile information was stored in the database by digitizing the tomography of the refraction seismic test lines. An outlier analysis technique based on cross-validation was adopted to detect the outliers, i.e., spatially unbiased and extreme values, in the borehole information, and 10% of the

boreholes were excluded from the spatial interpolation. The target of the spatial interpolation, i.e., the 3D volume of the original ground in the construction, was defined as an unstructured grid and produced using a DEM.

An integration analysis method for the borehole and geophysical test data was developed for the geostatistical interpolation of the subsurface geo-layer. A site-specific $V_P$ was derived locally for each geo-layer by supplementing and renewing the integration method developed by Kim *et al.* (2016). In contrast to the original integration method involving the use of IK, which is complex, OK and SGS were applied in this study. The analysis results obtained via an interpolation method with good prediction performance can be selectively employed to formulate a site-specific correlation between the geo-layer strata and $V_P$ with consideration of the separation distance. On attempting to confirm the reliability by introducing three test boreholes, the prediction result of the original method was found to be more accurate than that of the proposed method in the case of one test borehole. However, the reliability of the proposed integration method was improved according to a comparison of the overall RMSE. In particular, the proposed method's prediction of the depth to the weathered rock layer at the construction site was accurate to approximately over 1 m.

A geostatistical optimization method was developed and applied to the 3D modeling of the SPT-N value. Geostatistical optimization involves the quantitative evaluation of the reliability of multiple realizations, as the result of a conditional simulation, using cross-validation and the selection of only the realizations having a high accuracy. We obtained the 3D SPT-N value that satisfied the user-defined prediction performance with an error of <0.5. Reliability tests of the geostatistical optimization with two random boreholes indicated that the optimized SGS-based method reproduced the SPT-N value of the original subsurface better than conventional geostatistical methods. In future research, the prediction reliability should be evaluated according to the resolution of the unstructured grid target volume, and a parametric study of the geostatistical optimization variables should be conducted.

## Acknowledgments

## References

ASTM (2002), *Standard Test Method for Penetration Test and Splitbarrel Sampling of Soils*, American Society of Testing and Materials, Philadelphia, PA, USA.

ASTM (2019), *Standard Guide for Contents of Geostatistical Site Investigation Report*, American Society of Testing and Materials: Philadelphia, PA, USA.

Boschetti, F., Dentith, M.C. and List, R.D. (1996), "Inversion of seismic refraction data using genetic algorithms", *Geophysics*, **61**(6), 1715-1727. https://doi.org/10.1190/1.1444089.

Chen, G., Zhu, J., Qiang, M. and Gong, W. (2018), "Three-dimensional site characterization with borehole data–a case study of Suzhou area", *Eng. Geol.*, **234**, 65-82. https://doi.org/10.1016/j.enggeo.2017.12.019.

Ching, J. and Phoon, K.K. (2014), "Correlations among some clay parameters—the multivariate distribution", *Can. Geotech. J.*, **51**, 686-704. https://doi.org/10.1139/cgj-2013-0353.

Daya, A.A. and Bejari, H. (2015), "A comparative study between simple kriging and ordinary kriging for estimating and modeling the Cu concentration in Chehlkureh deposit, SE Iran", *Arabian J. Geosci.*, **8**(8), 6003-6020. https://doi.org/10.1007/s12517-014-1618-1.

De-fu, C., Li-xin, W. and Zuo-ru, Y. (2008), "3D Urban Geological Modeling and its Application in China: Technologies and Developments", *Proceedings of the IGARSS 2008-2008 IEEE International Geoscience and Remote Sensing Symposium*, Boston, MA, USA, July.

De Rienzo, F., Oreste, P. and Pelizza, S. (2008), "Subsurface geological-geotechnical modelling to sustain underground civil planning", *Eng. Geol.*, **96**(3-4), 187-204. https://doi.org/10.1016/j.enggeo.2007.11.002.

Delfiner, P. (1976), "Linear estimation of non stationary spatial phenomena", *Advanced geostatistics in the mining industry*, Rome, Italy, October.

Gallerini, G. and De Donatis, M. (2009), "3D modeling using geognostic data: The case of the low valley of Foglia river (Italy)", *Comput. Geosci.*, **35**, 146-164. https://doi.org/10.1016/j.cageo.2007.09.012.

Gómez-Hernández, J.J. and Srivastava, R.M. (1990), "ISIM3D: An ANSI-C three-dimensional multiple indicator conditional simulation program", *Comput. Geosci.*, **16**, 395-440. https://doi.org/10.1016/0098-3004(90)90010-Q.

Guarascio, M., David, M. and Huijbregts, C. (1976). *Advanced geostatistics in the mining industry*, D. Proc. of the NATO ASI, Reidel Publ., Dordrecht, The Netherlands.

Haeni, F. (1986), "Application of seismic refraction methods in groundwater modeling studies in New England", *Geophysics*, **51**, 236-249. https://doi.org/10.1190/1.1442083.

Han, L., Wang, L., Ding, X., Wen, H., Yuan, X. and Zhang, W. (2022), "Similarity quantification of soil parametric data and sites using confidence ellipses", *Geosci. Front.*, **13**(1), https://doi.org/10.1016/j.gsf.2021.101280.

Han, L., Wang, L., Zhang, W., Geng, B. and Li, S. (2021), "Rockhead profile simulation using an improved generation method of conditional random field", *J. Rock Mech. Geotech. Eng.*, **14**(3), 896-908, https://doi.org/10.1016/j.jrmge.2021.09.007.

Huang, L., Cheng, Y.M., Leung, Y.F. and Li, L. (2019), "Influence of rotated anisotropy on slope reliability evaluation using conditional random field", *Comput. Geotech.*, **115**, 103-133. https://doi.org/10.1016/j.compgeo.2019.103133.

Isaaks, E. and Srivastava, R. (1989), *An introduction to applied geostatistics*, Oxford University Press, New York, NY, USA.

Kim, H.S., Kim, H.K., Shin, S.Y. and Chung, C.K. (2012), "Application of statistical geo-spatial information technology to soil stratification in the Seoul metropolitan area", *Georisk: Assessment and Management of Risk for Engineered Systems and Geohazards*, **6**(4), 221-228. https://doi.org/10.1080/17499518.2012.744248.

Kim, H.S., Chung, C.K. and Kim, H.K. (2016), "Geo-spatial data integration for subsurface stratification of dam site with outlier analyses", *Environ. Earth Sci.*, **75**, 168. https://doi.org/10.1007/s12665-015-4931-4.

Kim, M. (2020), "Optimization of Three-dimensional geostatistical integration of site investigation information", Ph.D. Dissertation, Seoul National University, Seoul, South Korea.

Kim, M., Kim, H.S. and Chung, C.K. (2020), "A three-dimensional geotechnical spatial modeling method for borehole dataset using optimization of geostatistical approaches", *KSCE J. Civil Eng.*, **24**, 778-793. https://doi.org/10.1007/s12205-020-1379-1.

Kocbay, A. and Kilic, R. (2006), "Engineering geological assessment of the Obruk dam site (Corum, Turkey)", *Eng. Geol.*, **87**(3-4), 141-148. https://doi.org/10.1016/j.enggeo.2006.04.005.

Koltermann, C.E. and Gorelick, S.M. (1996), "Heterogeneity in sedimentary deposits: A review of structure-imitating, process-imitating, and descriptive approaches", *Water Resour. Res.*, **32**, 2617-2658. https://doi.org/10.1029/96WR00025.

Kupfersberger, H. and Deutsch, C.V. (1999), "Methodology for integrating analog geologic data in 3-D variogram modeling", *AAPG bulletin*, **83**, 1262-1278.

Leuangthong, O., McLennan, J.A. and Deutsch, C.V. (2004), "Minimum acceptance criteria for geostatistical realizations", *Nat. Resour. Res.*, **13**(3), 131-141. https://doi.org/10.1023/B:NARR.0000046916.91703.bb.

Liu, D., Liu, H., Wu, Y., Zhang, W., Wang, Y. and Santosh, M. (2022), "Characterization of geo-material parameters: Gene concept and big data approach in geotechnical engineering", *Geosyst. Geoenviron.*, **1**(1), https://doi.org/10.1016/j.geogeo.2021.09.003.

Li, X., Cheng, G. and Lu, L. (2000), "Comparison of spatial interpolation methods", *Adv. Earth Sci.*, **15**(3), 260-265. https://doi.org/10.11867/j.issn.1001-8166.2000.03.0260.

Li, J., Cassidy, M.J., Huang, J., Zhang, L. and Kelly, R. (2016), "Probabilistic identification of soil stratification", *Géotechnique*, **66**(1), 16-26. https://doi.org/10.1680/jgeot.14.P.242.

Murakami, S., Yasuhara, K., Suzuki, K. and Komine, H. (2006), "Reliable land subsidence mapping using a spatial interpolation procedure based on geostatistics", *Soils Found.*, **46**(2), 123-134. https://doi.org/10.3208/sandf.46.123.

Oh, S., Chung, H. and Lee, D.K. (2004), "Geostatistical integration of MT and borehole data for RMR evaluation", *Environ. Geol.*, **46**, 1070–1078. https://doi.org/10.1007/s00254-004-1115-z.

Osterholt, V. and Dimitrakopoulos, R. (2018), *Simulation of orebody geology with multiple-point geostatistics—application at Yandi channel iron ore deposit, WA, and implications for resource uncertainty*, In Advances in applied strategic mine planning (pp. 335–352). Springer, Cham.

Phoon, K.-K., Ching, J. and Shuku, T. (2021), "Challenges in data-driven site characterization", *Georisk: Assessment and Management of Risk for Engineered Systems and Geohazards*, **1**(13), https://doi.org/10.1080/17499518.2021.1896005.

Phoon, K.K. and Kulhawy, F.H. (1999), "Characterization of geotechnical variability", *Can. Geotech. J.*, **36**(4), 612-624. https://doi.org/10.1139/t99-038.

Pinheiro, M., Vallejos, J., Miranda, T. and Emery, X. (2016), "Geostatistical simulation to map the spatial heterogeneity of geomechanical parameters: A case study with rock mass rating", *Eng. Geol.*, **205**, 93-103. https://doi.org/10.1016/j.enggeo.2016.03.003.

Seoul Metropolis (2006), *Geotechnical investigation handbook*, Seoul Metropolis, Seoul.

Sotiropoulos, N., Benardos, A. and Mavrikos, A. (2016), "Spatial modelling for the assessment of geotechnical parameters", *Procedia Eng.*, **165**, 334-342. https://doi.org/10.1016/j.proeng.2016.11.708.

Wackernagel, H. (2003), *Multivariate Geostatistics: An Introduction with Applications*, Springer Science & Business Media.

Wang, J., Schweizer, D., Liu, Q., Su, A., Hu, X. and Blum, P. (2021), "Three-dimensional landslide evolution model at the Yangtze River", *Eng. Geol.*, **292**, 106275. https://doi.org/10.1016/j.enggeo.2021.106275.

Webster, R., Oliver, M.A. (2007), *Geostatistics for environmental scientists*, John Wiley & Sons.

Weissmann, G.S., Carle, S.F. and Fogg, G.E. (1999), "Three-dimensional hydrofacies modeling based on soil surveys and transition probability geostatistics", *Water Resour. Res.*, **35**, 1761-1770. https://doi.org/10.1029/1999WR900048.

Xu, J., Zhang, L., Li, J., Cao, Z., Yang, H. and Chen, X. (2021), "Probabilistic estimation of variogram parameters of geotechnical properties with a trend based on Bayesian inference using Markov chain Monte Carlo simulation", *Georisk: Assessment and Management of Risk for Engineered Systems and Geohazards*, **15**(2), 83-97. https://doi.org/10.1080/17499518.2020.1757720.

Zhao, T. and Wang, Y. (2020), "Non-parametric simulation of non-stationary non-gaussian 3D random field samples directly from sparse measurements using signal decomposition and Markov Chain Monte Carlo (MCMC) simulation", *Reliab. Eng. Syst. Saf.*, **203**. https://doi.org/10.1016/j.ress.2020.107087.

Zhang, J., Huang, H.W. and Phoon, K.K. (2013), "Application of the Kriging-Based Response Surface Method to the System Reliability of Soil Slopes", *J. Geotech. Geoenviron. Eng.*, **139**(4), 651–655. https://doi.org/10.1061/(ASCE)GT.1943-5606.0000801.

Zelt, C.A. and Barton, P.J. (1998), "Three-dimensional seismic refraction tomography: A comparison of two methods applied to data from the Faeroe Basin", *J. Geophys.Res.: Solid Earth*, **103**, 7187-7210. https://doi.org/10.1029/97JB03536.

*IC*